

Photoluminescence and Conductivity of Self-Assembled π - π Stacks of Perylene Bisimide Dyes

Zhijian Chen,^[a] Vladimir Stepanenko,^[a] Volker Dehm,^[a] Paulette Prins,^[b] Laurens D. A. Siebbeles,^[b] Joachim Seibt,^[c] Philipp Marquetand,^[c] Volker Engel,^[c] and Frank Würthner*^[a]

Dedicated to Professor Klaus Müllen on the occasion of his 60th birthday

Abstract: The self-assembly of a new, highly fluorescent perylene bisimide dye **2** into π stacks, both in solution and condensed phase, has been studied in detail by NMR spectroscopy, vapor pressure osmometry (VPO), UV/Vis and fluorescence spectroscopy, differential scanning calorimetry (DSC), optical polarizing microscopy (OPM) and X-ray diffraction. The NMR and VPO measurements revealed the formation of extended π - π stacks of the dye molecules in solution. The aggregate size determined from VPO and DOSY NMR measurements agree well with that obtained from the concentration and temperature-dependent UV/Vis

spectral data by employing the isodesmic model (equal K model). In the condensed state, dye **2** possesses a hexagonal columnar liquid crystalline (LC) phase as confirmed by X-ray diffraction analysis. The columnar stacking of this dye has been further explored by atomic force microscopy (AFM). Well-resolved columnar nanostructures of the compound are observed on graphite surface. A color-tunable luminescence from green to red has been ob-

served upon aggregation which is accompanied by an increase of the fluorescence lifetime and depolarization. The observed absorption properties can be explained in terms of molecular exciton theory. The charge transport properties of dye **2** have been investigated by pulse radiolysis-time resolved microwave conductivity measurements and a 1D charge carrier mobility up to $0.42 \text{ cm}^2 \text{ V}^{-1} \text{ s}^{-1}$ is obtained. Considering the promising self-assembly, semiconducting, and luminescence properties of this dye, it might serve as a useful functional material for nano-(opto)electronics.

Keywords: charge carrier mobility • dyes/pigments • liquid crystals • perylene bisimide • self-assembly


Introduction

Functional dye assemblies possessing energy and charge transport properties have attracted considerable attention in materials as well as in biological sciences in the past years.^[1] Inspired by the pivotal role of self-assembled chlorophyll dyes in the photosynthesis of green plants,^[2] efforts have been devoted to the rational control of the self-assembly process of artificial functional dyes in particular with respect to applications in organic electronic devices. For example, columnar liquid-crystalline and amphiphilic tubule-forming hexabenzocoronenes have been successfully prepared that exhibit promising optical and electrical properties.^[3] Furthermore, well-ordered multi-component assemblies of p- and n-type semiconducting π -electron systems have been constructed for efficient charge carrier separation upon illumination.^[4]

[a] Z. Chen, V. Stepanenko, V. Dehm, Prof. F. Würthner
Universität Würzburg, Institut für Organische Chemie
and Röntgen Research Center for Complex Material Systems
Am Hubland, 97074 Würzburg (Germany)
Fax: (+49) 931-888-4756
E-mail: wuerthner@chemie.uni-wuerzburg.de

[b] P. Prins, Prof. L. D. A. Siebbeles
Opto-electronic Materials Section, DelftChemTech
Delft University of Technology
2628 BL Delft (The Netherlands)

[c] J. Seibt, P. Marquetand, Prof. V. Engel
Universität Würzburg, Institut für Physikalische Chemie
Am Hubland, 97074 Würzburg (Germany)

 Supporting information for this article is available on the WWW under <http://www.chemeurj.org/> or from the author: Additional spectroscopic data, aggregation studies and other measurements of PBI **2**.

Among functional dyes, perylene tetracarboxylic acid bisimides (PBIs) have been investigated quite intensively^[5] due to their favorable properties, such as light fastness, intense photoluminescence,^[6] and outstanding n-type semiconductivity.^[7] Thus, these dyes and their assemblies find application as functional units in artificial light harvesting systems,^[8] photoinduced electron transfer systems,^[9] and organic electronic devices such as organic light emitting diodes (OLED),^[10] organic thin-film transistors (OTFT),^[11] and solar cells.^[12] Different types of intermolecular forces such as hydrogen bonding, π - π stacking and metal-ligand interactions have been applied to direct the formation of desirable supramolecular structures of PBIs.^[5] Among these non-covalent interactions, π - π stacking plays an important role in the self-assembly of PBI dyes and can determine the texture of thin films prepared by solution processible techniques such as spin-coating or zone-casting for device fabrication.^[13] In some cases it has been shown that π stacks can be transferred on substrates by simple solution casting method.^[14] Another important property of PBIs that is determined by π - π stacking is their thermotropic or lyotropic liquid crystallinity,^[15] which leads to the formation of columnar dye stacks that can enable 1D charge carrier mobility.^[16] It has been found that in such liquid crystalline (LC) phase, the transport of charge carriers along the column axis is several orders of magnitude faster than that in perpendicular direction.^[17]

In general, the liquid crystallinity of polyaromatic compounds arises from micro-segregation of a large-size rigid aromatic core and flexible, non-bulky alkyl chains.^[18] In our previous work,^[15a] tridodecyloxyphenyl groups were introduced at the imide positions of a PBI to obtain the LC PBI dye **1** (Scheme 1) which exhibits high charge carrier mobility.^[15d] However, neither in monomeric nor in aggregated state is dye **1** fluorescent. Noteworthy, fluorescence quench-

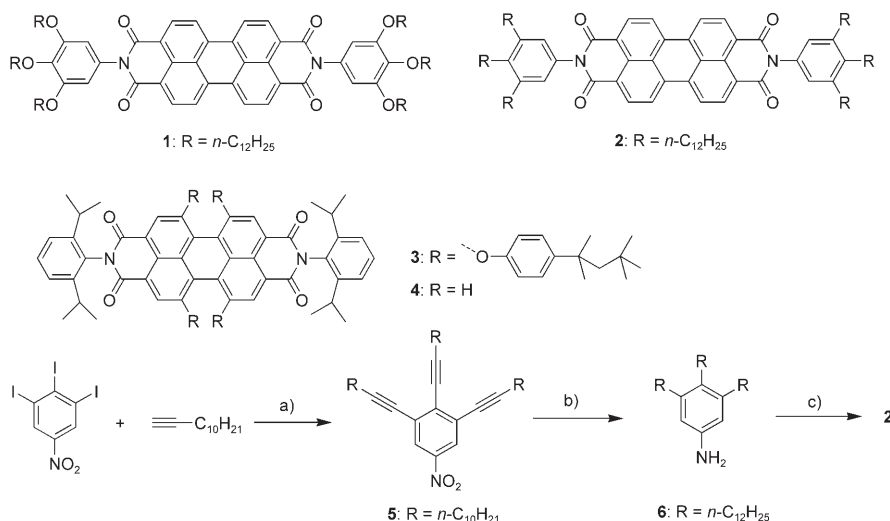
ing was also observed for a calix[4]arene-functionalized PBI derivative, which contains alkoxyphenyl groups at imide positions.^[19] The fluorescence quenching in these chromophores is attributed to photoinduced electron transfer from the electron-rich alkoxyphenyl groups to the perylene bisimide unit.^[15a,20] In contrast, recently we have observed that PBI dye **2** (Scheme 1), which contains trialkylphenyl groups, instead of trialkoxyphenyl groups at the imide positions, and its aggregates exhibit unique fluorescence properties.^[21] Here we present our detailed investigations on self-assembly, both in solution and condensed state (liquid crystallinity), of PBI dye **2**, and report on optical and charge transport properties of its π - π -stacked aggregates.

Results and Discussion

Synthesis: The synthesis of the trialkylphenyl-functionalized PBI **2** was achieved in three steps (Scheme 1). First, the precursor **5** was synthesized according to Sonogashira coupling reaction^[22] between 1-dodecyne and 3,4,5-triiodonitrobenzene^[23] in 90% yield. Subsequent reduction of the triple bonds and the nitro group of **5** was accomplished by Pd-catalyzed hydrogenation to give aniline **6**. Finally, the condensation of **6** with perylene tetracarboxylic bisanhydride in the presence of $\text{Zn}(\text{OAc})_2$ as catalyst^[24] afforded the desired PBI **2**, which was fully characterized by ^1H NMR spectroscopy, MS spectrometry, and elemental analysis. The PBIs **3** and **4** were used as reference compounds.^[25]

Temperature and concentration-dependent aggregate formation in solution: The aggregation behavior of PBI **2** was first studied by temperature-dependent ^1H NMR spectroscopy. In CDCl_3 solution, a simple pattern of sharp signals for the perylene protons was observed, indicating that the compound is in monomeric form in this polar solvent (Figure 1).

However, when it was measured in nonpolar deuterated methylcyclohexane ($[\text{D}_{14}]\text{MCH}$), drastic changes compared with the spectrum in CDCl_3 were observed, apparently due to aggregation. In $[\text{D}_{14}]\text{MCH}$ at 299 K, the spectrum displayed a large number of signals that overlap with each other in the range between 9.2 to 6.5 ppm due to different aggregated species. The complex pattern of the spectrum and high or low-field shift of proton signals, compared with those of monomeric species, can be interpreted in terms of shielding or deshielding of the protons by π systems of



Scheme 1. Chemical structures of the trialkoxyphenyl-containing PBI dye **1**,^[15a] trialkylphenyl-functionalized PBI **2**, and the two reference PBIs **3** and **4**.^[25] Synthesis of PBI **2**: a) $[\text{Pd}(\text{PPh}_3)_2\text{Cl}_2]$, CuI , Et_3N , 80°C ; 4 h, 90%. b) H_2 , Pd/C , EtOH/EtOAc ; RT, 24 h, 53%. c) Perylene-3,4,9,10-tetracarboxylic acid bisanhydride, $\text{Zn}(\text{OAc})_2$, quinoline, 180°C , 2 h, 56%.

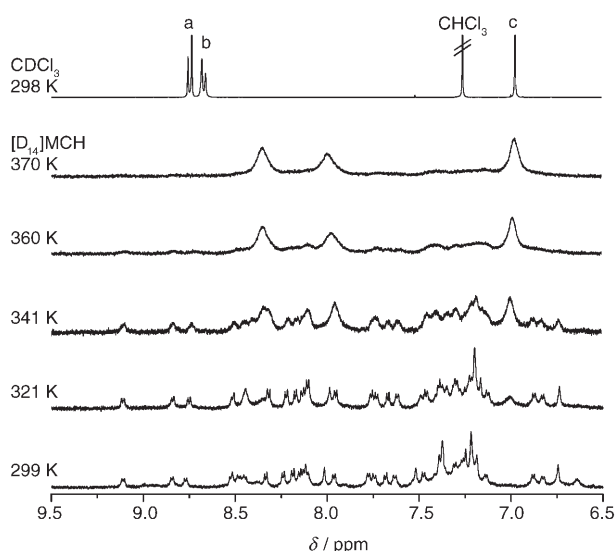


Figure 1. Temperature-dependent 600 MHz ^1H NMR spectra of PBI **2** (1.1×10^{-3} M) in $[\text{D}_{14}]\text{MCH}$ at 299 to 370 K and in CDCl_3 at 298 K. (The signals labeled as a, b are assigned to perylene ring protons and signal c to the protons of phenyl groups at imide positions.)

neighboring dye molecules that are stacked closely in aggregates (could be as close as 3.4 \AA according to the crystal structures of unsubstituted PBIs^[5]). The ^1H NMR spectra observed for **2** in $[\text{D}_{14}]\text{MCH}$ are significantly different from those reported for a related PBI derivative in CDCl_3 where fast exchange between monomer and aggregates took place.^[26] In the latter case, the spectra were of simple pattern that are comparable with those of monomer species and only high-field shifts of the perylene proton signals were observed. Thus, the complex spectral pattern of **2** in $[\text{D}_{14}]\text{MCH}$ at 299 K indicates that the formed aggregates are kinetically relatively stable on NMR time scale at this temperature. Upon gradual increase of temperature from 299 to 360 K, the sharp signals of aggregates at 299 K have increasingly broadened and at 370 K (near the boiling point of the solvent) the spectrum displayed a relatively simple pattern with three broad signals. One of them appears at 7.0 ppm which corresponds to the chemical shift for imide phenyl protons in the monomer and the remaining two high-field shifted signals belong to perylene protons. These spectral changes indicate the “melting” of the aggregates. At higher temperatures than RT, more rapid exchanges between monomer and aggregated species take place and only averaged proton signals can be observed, as the spectrum at 370 K shows. Furthermore, in the concentration-dependent ^1H NMR spectra of **2** in $[\text{D}_{14}]\text{MCH}$ at 298 K (Figure S1 in the Supporting Information), gradual changes in spectral shape and an increase of signal number for aromatic protons were observed with increasing concentration of **2**. These temperature and concentration-dependent NMR studies reveal formation of π - π -stacked oligomeric aggregates of PBI **2** in nonpolar MCH.

To further substantiate the formation of extended PBI **2** aggregates in solution, DOSY (diffusion ordered spectro-

py) NMR experiments were performed.^[27] The translational diffusion coefficient D [m^2s^{-1}] of molecular species can be estimated by the Stokes-Einstein equation: $D = k_B T / (6\pi\eta R)$, where T is the temperature, η is the viscosity of the solvent, R is the hydrodynamic radius of the molecule or assembly and k_B is the Boltzmann constant. According to this equation, the D value is inversely proportional to the hydrodynamic radius (R) of a molecule. Thus, the size of species could be compared based on their diffusion coefficients when the other parameters are identical. For PBI **2**, only a single apparent diffusion coefficient was observed at different concentrations for all the aggregated species. The same observation was made in a recent DOSY NMR study on the aggregation of proteins and was interpreted as a result of ensemble averaging of the diffusion coefficients of different species on macroscopic scale.^[28] Such averaging could also be feasible for monomer-dimer equilibrium or equilibria involving higher aggregated species.^[29] If only monomer-dimer equilibrium exists, the D values for both monomer and dimer species should be nearly identical, as shown by our previous studies on a coordination dimer of terpyridine-substituted perylene bisimide.^[30] On the other hand, for highly aggregated species which have much larger R values than monomers, obviously, a change of D values should be observable on DOSY NMR spectra.

As the monomeric form of **2** can only be obtained at very low concentrations (see UV/Vis studies), a reference PBI **3**, which has a nearly identical molecular mass (1528 g mol^{-1}) as **2** (1552 g mol^{-1}) and does not aggregate owing to its extremely bulky substituents (verified by UV/Vis spectroscopy and VPO at $10^{-2} \text{ mol L}^{-1}$ in MCH), was used for comparison. For all the aromatic signals of **2**, D value of $1.57 \times 10^{-10} \text{ m}^2\text{s}^{-1}$ was observed at a concentration of $1.1 \times 10^{-3} \text{ M}$ (Figure S2 in the Supporting Information), while the reference compound **3** showed diffusion coefficient of $3.40 \times 10^{-10} \text{ m}^2\text{s}^{-1}$ at $1.3 \times 10^{-3} \text{ M}$. The large difference between the D values of **2** and monomeric **3** indicates that the hydrodynamic radius of the present species of **2** is much higher than that of the reference compound. These data clearly indicate formation of extended aggregates of dye **2** in MCH. Furthermore, a gradual decrease of the D value from $1.57 \times 10^{-10} \text{ m}^2\text{s}^{-1}$ to $7.36 \times 10^{-11} \text{ m}^2\text{s}^{-1}$ was observed, when the concentration of the solution was increased from 1.1×10^{-3} to 0.11 M (Figure 2), indicating the increase of the hydrodynamic radius of the aggregates.

This diffusion method can also provide the average aggregation number per stack as the cube root of molecular weight of aggregates has been suggested to be proportional with D^{-1} by simplistically taking all oligomers to be hydrodynamically spherical.^[27,31] Thus, the average aggregate size of **2** can be estimated as $N_{\text{DOSY}} \approx (D_{\text{ref}}/D)^3$, since the difference of the molecular mass of **2** and reference compound **3** is negligible, where D_{ref} and D are the translational diffusion coefficients obtained from DOSY NMR measurements for reference compound **3** and PBI **2**, respectively. It is worth to note that this estimation is only an approximate approach since the hydrodynamic shape of the aggregates deviates

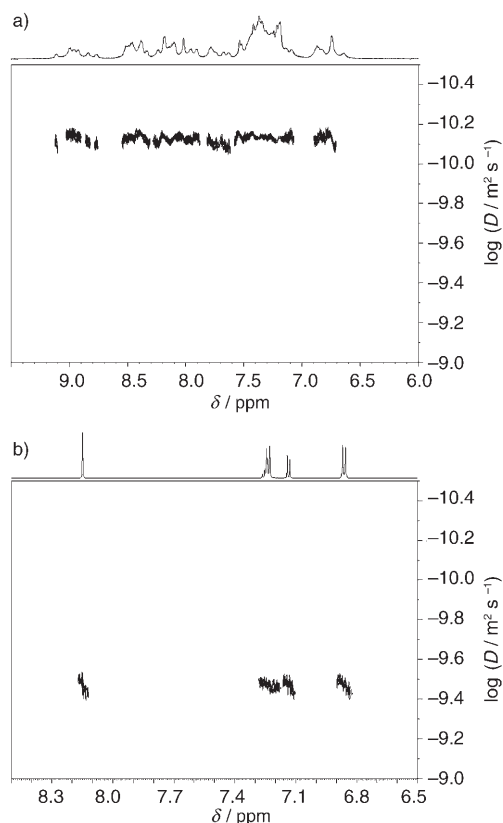


Figure 2. DOSY NMR spectra of a) PBI **2** at $c = 0.11$ M and b) the reference compound **3** at $c = 1.3 \times 10^{-3}$ M in $[D_{14}]$ MCH. The diffusion coefficients D [$\text{m}^2 \text{s}^{-1}$] are plotted in a logarithmic scale against chemical shift δ [ppm].

from spherical shape. The average numbers of aggregated dye **2** were estimated at three different concentrations and are given in Table 1.

Table 1. Average number of aggregated molecules N of PBI **2** at different concentrations and temperatures obtained from DOSY, VPO and UV/Vis spectroscopic measurements.

T [$^{\circ}\text{C}$]	c_T [mol L^{-1}]	N_{VPO}	N_{DOSY}	$N_{\text{UV/Vis}}$
25	1.1×10^{-3}		10	10
25	2.2×10^{-2}		20	42
25	1.1×10^{-1}		99	93
40	5.0×10^{-3}	9		11
50	5.0×10^{-3}	7		8
60	5.0×10^{-3}	6		6

Owing to the strong convection effect at higher temperatures in solution, it is difficult to obtain the DOSY spectra at higher temperatures. Therefore, temperature-dependent aggregation of **2** was studied by vapor pressure osmometry (VPO), which is based on the colligative properties and provides average molecular weight of the aggregates formed. At 40, 50, and 60°C and a concentration of $5.0 \times 10^{-3} \text{ M}^{-1}$, average molecular weight of 1.4×10^4 , 1.1×10^4 , and 9×10^3 Dalton were obtained, respectively, which correspond to

average aggregate sizes of 9, 7, and 6 aggregated molecules, respectively, for dye **2**. The results of DOSY NMR and VPO experiments confirm convincingly that in MCH extended aggregates of **2**, rather than dimer, are preferentially formed at different concentrations and temperatures.

To obtain more insight into the thermodynamics of the aggregation process of PBI **2**, concentration and temperature-dependent UV/Vis spectroscopic studies were performed. At very low concentrations (non-aggregated state), the UV/Vis spectra (Figure 3) displayed absorption bands between 400 and 550 nm for the S_0-S_1 transition of the PBI chromophore with $\lambda_{\text{max}} = 517$ nm and well-resolved vibronic structure that can be ascribed to the breathing vibration of the perylene skeleton which strongly coupled with the S_0-S_1 transition polarized along the long axis of the molecules.^[32] Upon increasing the concentration, the apparent absorption coefficients decrease gradually and the spectra become broader and less structured, reflecting the electronic coupling between the chromophores. Furthermore, a hypochro-

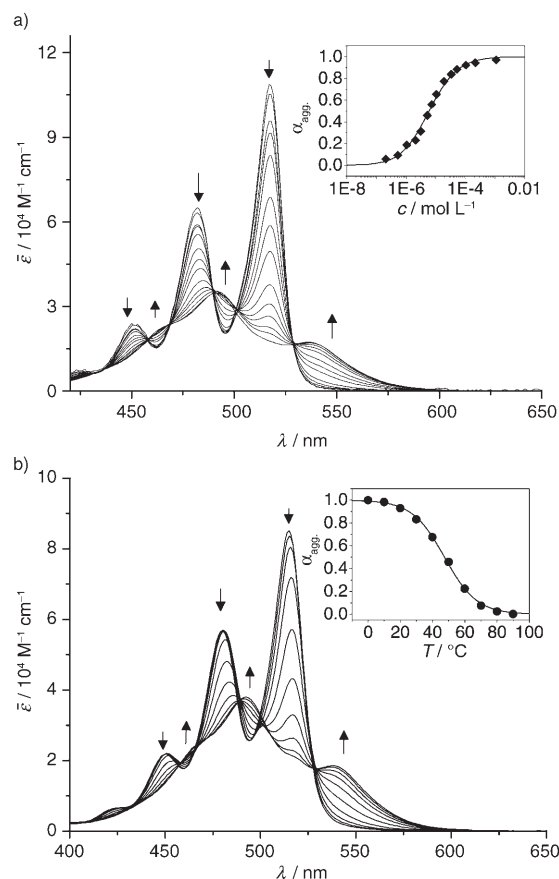


Figure 3. a) Concentration-dependent UV/Vis absorption spectra of PBI **2** (2.1×10^{-7} to 1.1×10^{-3} M) in MCH at room temperature. Arrows indicate the changes upon increasing the concentration. Inset: Fraction of aggregated molecules α_{agg} for PBI **2** as a function of concentration in MCH obtained by fitting the apparent absorption coefficients at $\lambda = 517$ nm to the isodesmic model. b) Temperature-dependent UV/Vis absorption spectra of **2** from 0 to 90°C (5.0×10^{-4} M). Arrows indicate the changes upon decreasing the temperature (90 to 0°C). Inset: α_{agg} of **2** versus temperature.

mic shift of λ_{\max} of about 27 nm (1000 cm^{-1}) and a progressive evolution of a new broad bathochromically shifted band at 538 nm is observed. At 490 and 529 nm, there appear to be isosbestic points, which, however, shift slightly from 490 to 492 nm and 529 to 531 nm upon increasing concentration. These spectral features are highly indicative for the formation of face-to-face stacked dye aggregates.

In general, the π - π stacking of disk-shaped molecules generates one-dimensional aggregates reversibly in solution and the aggregation behavior can be ascribed to the strong π - π interactions among discotic molecules. Such open-ended linear aggregates are usually polydisperse and their formation can be described by equal K or isodesmic chemical equilibria,^[33] in which a constant K value is assumed for all the binding processes. Nonlinear least-square regression analysis of the concentration-dependent UV/Vis spectral data showed that the aggregation behavior can be well described by this model. The value of K at room temperature was determined as $9.7 \times 10^4\text{ L mol}^{-1}$, which is about two orders of magnitude smaller than that of the previously reported structurally similar PBI dye **1**^[15a] in same solvent, indicating that the chemical nature of the substituents play an important role in the aggregation strength.

In the temperature-dependent UV/Vis spectra of **2** (Figure 3b), the spectral changes are highly comparable with those observed in concentration-dependent measurements. A "melting" temperature^[34] of 47 °C was calculated for the phase transition from aggregated dyes to molecularly dissolved species for **2**. Temperature-dependent UV/Vis spectra of dye **2** were recorded at different concentrations and aggregation constants K were determined at seven different temperatures (Table S1, Supporting Information). The enthalpy and entropy contributions to the Gibbs free energy changes for the aggregation of **2** were evaluated from a van't Hoff plot (Figure 4). A plot of $\ln K$ versus T^{-1} shows a perfectly linear relationship (correlation coefficient 0.999) and the standard enthalpy and entropy are determined to be $\Delta H^\circ = -56.3 \pm 1.1\text{ kJ mol}^{-1}$ and $\Delta S^\circ = -95.8 \pm 3.6\text{ J mol}^{-1}\text{ K}^{-1}$. The negative enthalpy and entropy values indicate that the self-assembly process is enthalpy driven.

Based on isodesmic model, the molar fractions of n -mer aggregates α_n and the average dye numbers per stack N

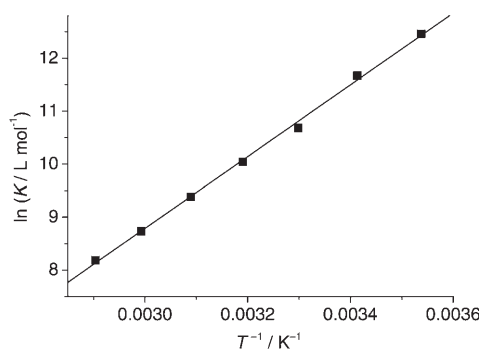


Figure 4. Van't Hoff plot for the temperature dependence of the aggregation constant K of **2** in MCH.

(average aggregation number) at different concentrations and temperatures can be calculated from the equations 1 and 2, respectively, where K is the aggregation constant and c_T is the concentration of **2**. From these equations, the average numbers of aggregated dyes versus concentration at different temperatures were calculated (Figure 5). The obtained values are shown in Table 1 and they are in good agreement with those determined from DOSY and VPO measurements.

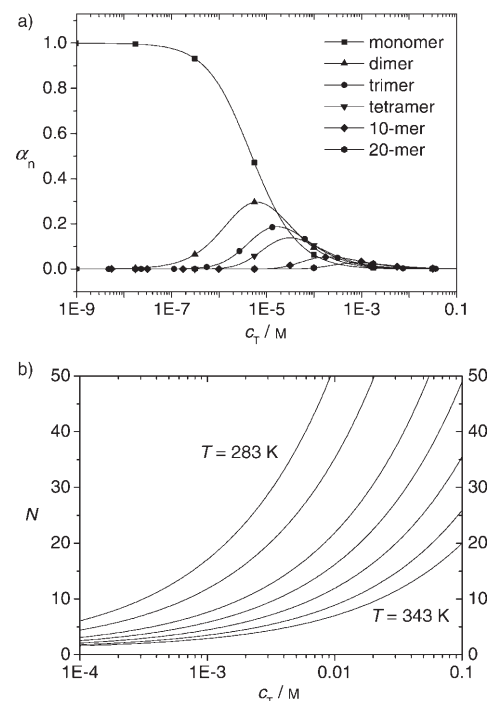


Figure 5. a) Molar fraction of n -mer aggregates α_n of PBI **2** as a function of total concentration c_T . b) Calculated average aggregation size N of **2** versus total concentration c_T at different temperatures from 283 to 343 K with 10 K interval.

$$\alpha_n = nc_T^{n-1}K^{n-1} \left(\frac{2Kc_T + 1 - \sqrt{4Kc_T + 1}}{2K^2c_T^2} \right)^n \quad (1)$$

$$N = \frac{1}{2}(1 + \sqrt{4Kc_T + 1}) \quad (2)$$

Although UV/Vis spectroscopy was performed at lower concentration range than for DOSY NMR and VPO measurements, the data summarized in Table 1 show that in most cases the aggregate size derived from UV/Vis spectroscopy at high concentrations agrees well with those determined from NMR and VPO measurements. Thus, a combination of different methods, such as UV/Vis spectroscopy, diffusion NMR and VPO, that have different concentration windows can be used to obtain a consistent picture for the formation of π - π -stacked assemblies, as convincingly demonstrated for dye **2** in nonpolar organic solvent.

Self-organization properties of dye 2 in condensed state:

Aggregation studies of dye **2** in solution (see above) have revealed strong π - π interactions among the dyes, thus, it is expected that this dye also possesses self-organizing properties in condensed state, that is, mesophase formation. Indeed, differential scanning calorimetry (DSC), optical polarizing microscopy as well as X-ray diffraction studies with the bulk samples of **2** unequivocally confirm liquid crystallinity (LC) of this dye. The DSC thermogram (Figure S3, Supporting Information) of this compound shows a crystal-LC phase transition with an endothermic peak at 85°C with $\Delta H = 71 \text{ J g}^{-1}$ (melting of the alkyl chains) and a LC phase-isotropic phase transition at 300°C with $\Delta H = 12 \text{ J g}^{-1}$. The clearing point of **2** is about 70°C lower than that observed for the trialkoxyphenyl-substituted PBI **1**. No subsequent recrystallization took place as no transitions corresponding to the first endothermic peak were observed on cooling and second heating, indicating that the recrystallization is kinetically suppressed.

Under the polarizing optical microscope, a dendritic texture was observed for the LC phase of **2** (Figure 6). The X-ray diffraction (XRD) measurements were performed for the bulk sample of **2** after cooling from 115°C to room temperature (Figure 7). The six observed Bragg reflections in the small angle region can be indexed according to a two-dimensional hexagonal lattice with satisfactory accuracy (Table S2 in the Supporting Information). The cell parameter of the hexagonal phase of **2** is 3.35 nm, which is nearly identical with that reported for the structurally similar dye **1** containing trialkoxyphenyl groups.^[15a] The diffused halo displayed at around 20° can be attributed to the disordered alkyl chains. The absence of sharp peak in this region reveals a disordered stacking along the column axis. Owing to the elongated nature of **2** and the fact that, generally, columnar hexagonal phases possess a circular cross-section, a rotational displacement of the individual dye units along the π - π -stacking direction in LC phase can be implied, as the model in Figure 8 shows. Molecular modeling study revealed a length of about 4.9 nm for compound **2** with fully extended conformation of the alkyl chains. The observed diameter of the column by X-ray analysis is 30% shorter. This can be attributed to the alkyl chain tail folding and interdigitating



Figure 6. Optical texture of dye **2** between two crossed polarizers obtained by cooling the sample from isotropic phase.

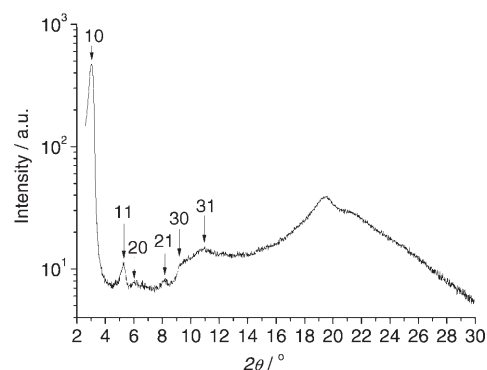


Figure 7. X-ray diffraction pattern for a sample of PBI **2** cooling from 115°C to RT with the Miller indices of the small angle diffraction peaks.

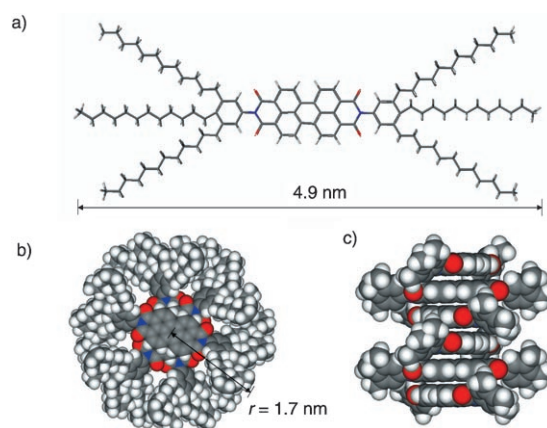


Figure 8. a) Molecular structure of PBI **2** with fully extended alkyl chains. b) Top view of a columnar stacking model of dye **2** with a rotational displacement of 60° of the molecular planes. c) Side view of the stack (for clarity phenyl groups, instead of trialkylphenyl groups, are shown in the molecules).

into neighboring columns, as pointed out by Percec et al. for other systems.^[35] In the lowest energy conformation of **2** that is assessed by molecular modeling, the two phenyl rings at imide positions are not co-planar with the perylene bisimide unit (Figure 8). Due to the bulkiness of the two phenyl rings, a rotation displacement is demanded for the π - π stacking of dye **2**.

The unique columnar stacking feature of PBI **2** was further verified by atomic force microscopy (AFM) studies. For this purpose, thin films were prepared by spin-coating of solution of PBI **2** on highly ordered pyrolytic graphite (HOPG). Tapping mode AFM images of the samples revealed multilayer structures (Figure 9a) with the height of 2.3 nm between the top and the adjacent layer. A high resolution image (Figure 9b) showed that the top layer is composed of long and bended columns which formed a fingerprint-like structure. Cross-section analysis of the lateral structure and 2D Fourier transformation of the AFM image revealed a mean value of $3.9 \pm 0.3 \text{ nm}$ for the distance between neighboring columns which is in good agreement with that observed by X-ray diffraction analysis for the liquid

crystal phase of **2**. When the thin film is prepared from CH_2Cl_2 solution, in which dye **2** is less aggregated, structures with much shorter rods were observed (Figure 9c), revealing the solvent effect on the topology of the thin film. Based on these results, a structure model of the aggregates is proposed in Figure 9e. According to this model, the height difference between the layers (2.3 nm) should be smaller than the diameter of the columns which is in agreement with our observations. As in the case of liquid crystal phase, the columns are segregated by the surrounding alkyl chains. The length of the columns ranges between 20 nm to several hundred nanometers which corresponds to columnar stacking of 60 to several thousand dye **2** molecules on graphite surface, assuming a π - π distance of 3.5 Å as observed previously in several crystal structures of *N,N'*-diphenyl PBI dyes.^[36]

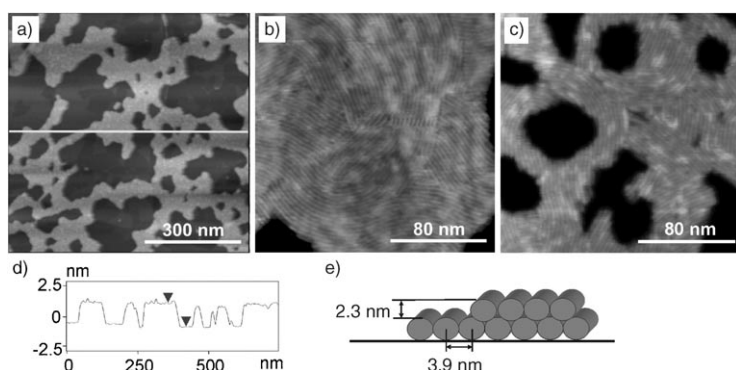


Figure 9. AFM images of thin films spin-coated from a solution of **2** onto HOPG: a) Topography image (from MCH solution, 4×10^{-4} M). b) High resolution topography image (from MCH solution, 4×10^{-4} M). c) High resolution topography image (from CH_2Cl_2 solution, 4×10^{-4} M). d) Cross-section analysis along the line in image a), and e) proposed model for the packing of columnar stacks on HOPG surface.

Optical properties of the aggregates of dye 2: Most of the reported crystal structures of PBI dyes show a parallel packing of molecules along the long molecular axis with longitudinal and transversal offsets between adjacent dyes.^[5] Only in very few cases rotational displacements that lead to a screw-type stacking of dyes have been found in crystals,^[5,36] as observed for the LC phase of the present dye **2**. As a consequence, novel optical and electrical properties might arise for the aggregates of dye **2**. In Figure 10a, the UV/Vis spectrum of a thin film of **2** (inset) and concentration-dependent fluorescence spectra of **2** in MCH solution and of a thin film as well are depicted. Remarkably, the absorption and the fluorescence spectra of PBI **2** in thin film match perfectly well with those obtained in high concentration in MCH (Figure 3). This is very indicative for similar packing features, in particular, with respect to the π - π stacking of the dye **2** in solution and in the condensed phase. Accordingly, not only XRD (columnar LC phase) and AFM (columns deposit from solution), but also optical spectroscopy (local contacts) provides evidence for identical or at least very similar arrangements for the aggregated dyes in solution, on surface and in the condensed state.

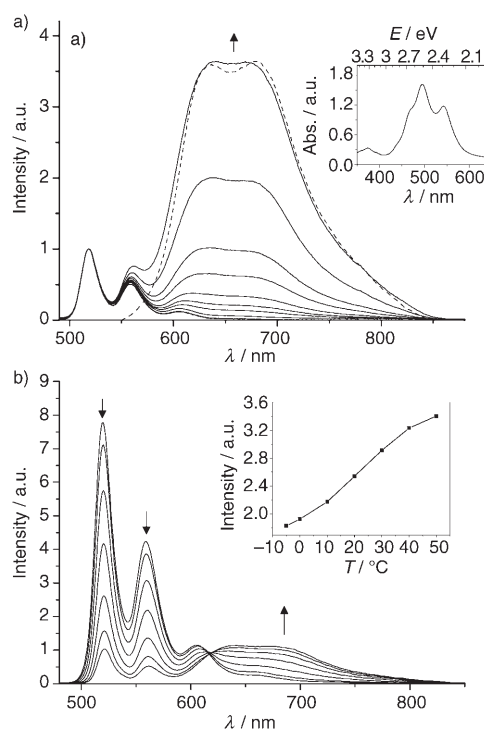


Figure 10. a) Concentration-dependent fluorescence spectra normalized at 518 nm (excited at the quasi-isosbestic point at 469 nm) of PBI **2** (2.1×10^{-7} M to 2.1×10^{-4} M) in MCH solution and solution-cast thin film (dashed line) at RT. The arrows indicate the changes upon increasing concentration. Inset: UV/Vis absorption spectrum of a spin-coated thin film of **2** annealed at 150 °C for 3 h. b) Temperature-dependent fluorescence spectra of **2** in *n*-hexane (1.0×10^{-6} M, excited at 469 nm) from -5 to 50 °C. The arrows indicate the changes upon decreasing temperature. Inset: The integrated fluorescence intensity of the sample at different temperatures.

The concentration-dependent fluorescence spectra of **2** (Figure 10a) display an emission band at 500–650 nm for the monomeric dye **2** with well-resolved vibronic structure at low concentrations ($< 10^{-6}$ M). Upon aggregation, a new broad band emerges at 600–850 nm (aggregate band) and its intensity increases strongly with increasing concentration. The long tail of this band reached the near infrared (NIR) region already at a concentration of 3×10^{-6} M. Taking into account that the monomer band is absent, the emission spectrum of a spin-coated thin film is very similar to that observed for concentrated solutions and only slightly shifted to lower energy (Figure 10a, dotted line). To shed more light into the fluorescence properties, temperature-dependent fluorescence spectroscopy studies were performed in the solvent *n*-hexane.^[37] For this solvent, the highest aggregation constant is given which enables the formation of aggregated species even in very dilute solution. Accordingly, at low temperatures the broad aggregate band at 600–850 nm can be observed together with the monomer band (Figure 10b). Upon increasing the temperature, this band is slightly hypsochromically shifted and the intensity gradually decreased. Simultaneously, the intensity of the monomer band increased

expectedly, indicating the transition of aggregates into monomeric species.

Remarkable color and intensity changes of the fluorescence were observed upon variation of concentration as well as temperature of the solution of **2**. In MCH, depending on the ratio of aggregated versus total dye molecules α_{agg} , the color of the fluorescence changed from green ($\alpha_{\text{agg}} < 0.3$, $N < 1.6$), to yellow ($\alpha_{\text{agg}} \approx 0.7$, $N \approx 2.3$), orange ($\alpha_{\text{agg}} \approx 0.8$, $N \approx 3.0$), red ($\alpha_{\text{agg}} > 0.9$, $N > 4.0$), and deep red (thin film) (Figure S4, Supporting Information). The fluorescence quantum yield Φ_{f} of **2** was determined as 0.63 in CH_2Cl_2 and 0.65 in MCH for highly dilute solutions, where only monomer band can be observed. Upon increasing the concentration, the fluorescence quantum yield decreased, although the fluorescence intensity increased continuously due to the higher concentration. By comparison of the observed fluorescence intensity with the non-aggregated reference PBI **4** ($\Phi_{\text{f}} = 1.0$ in MCH), the Φ_{f} of **2** at $1 \times 10^{-4} \text{ M}$ in MCH is estimated as 0.4 (see ref. [55]), which is about 60% of that observed for highly dilute solution (Figure S5, Supporting Information). Likewise, the decrease of the fluorescence intensity upon aggregation was also observed in the temperature-dependent fluorescence spectra (Figure 10b, inset). In *n*-hexane, at -5°C the intensity of the fluorescence decreased to about half of that at 50°C where only monomeric dyes are present. From these data, we can calculate a fluorescence quantum yield of 35% for the aggregates in *n*-hexane which is still a quite high value for an emitter in the red to near IR region.

To elucidate further the fluorescence properties of the dye **2** aggregates, fluorescence lifetime τ_{f} and anisotropy were measured for MCH solutions (Figures S6 and S7, Supporting Information). For a $2.5 \times 10^{-5} \text{ M}^{-1}$ solution of **2**, the fluorescence decays monitored at the monomer band (520 nm) and the aggregate band (650 nm) provided τ_{f} values of 3.2 ns and 32.7 ns, respectively. Thus, lifetime of the aggregate band is 10 times higher than that of the monomer band. Furthermore, fluorescence anisotropy was determined as 0.11 for the monomer band and 0.003 for the aggregate band. According to the theory, an anisotropy value as high as 0.4 is possible if no depolarization takes place neither by energy transfer processes to neighboring dyes nor by rotational diffusion. Practically, for low viscosity solvents the rotational diffusion of small fluorophores is fast and depolarization takes place. As mentioned, an anisotropy value of 0.11 was observed for dye **2** monomer in MCH. Upon aggregation, rotational diffusion should be slowed down due to the higher molecular mass of the dye aggregates. Thus, the anisotropy should increase if no other depolarization process takes place within the dye stacks. However, a nearly zero anisotropy value (0.003) was observed for the aggregate fluorescence band of dye **2**. This depolarization of the aggregate band can be explained in terms of efficient energy transfer among the stacked dyes. Due to their rotational displacement their transition dipoles are not parallel and the fluorescence polarization vanishes.

Most of the observed absorption properties of dye **2** can be rationalized by molecular exciton theory if rotational displacement in dye stacking is assumed.^[38] According to this theory, for *n* 1D π - π -stacked molecules each vibronic state in S_1 should split into a *n*-level band. Only the transitions to the top level (*H*-aggregates) or bottom level (*J*-aggregates) is allowed if all the transition dipoles are perfectly parallel to each other. Thus, compared with nonaggregated molecules, hypsochromic and bathochromic displacement of the absorption band can be observed in the electronic spectra for *H*- or *J*-aggregates, respectively. The hypsochromic shift of λ_{max} of **2** is indicative for the formation of cofacial (*H*-type) aggregates. However, when rotational displacements exist among the transition dipoles and the molecular vibration is strongly coupled with electronic transitions, as observed for compound **2**, the conventional selection rule does not apply anymore and the forbidden electronic transitions from the ground state to the lower excitonic state become partially allowed. Thus, both bathochromically and hypsochromically shifted absorption bands (related to λ_{max} of monomer) are observed for the dye **2** aggregates.

Theoretical calculations for aggregate spectra of face-to-face-stacked dimers of **2** with different rotation angles between the transition dipoles were performed^[39] based on established models.^[40] Basically, a single vibrational monomer mode is included and the dimer Hamiltonian is built from the monomer Hamiltonians within a single exciton picture, including a point-dipole coupling between the dimer excited states. Details of the model and time-dependent quantum calculations are given elsewhere.^[39] From a comparison between experimental and theoretical dimer absorption spectra, we have extracted a most likely dimer geometry, where the transition dipole moments of the monomers span an angle of $\beta = 55^\circ$ and the relative orientation of the dipole moments with respect to the monomer-monomer centre of mass vector has an angle of $\alpha_1 = \alpha_2 = 70^\circ$ (Figure 11). For this geometry, and an assumed monomer separation of 3.5 Å, the calculated absorption spectrum displayed in the

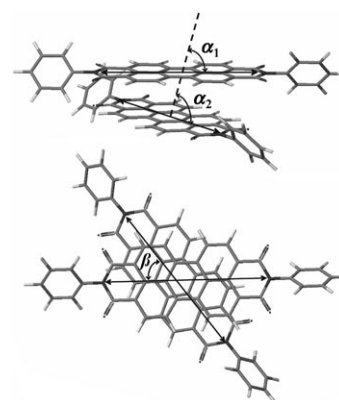


Figure 11. Dimeric stacking of **2** that provides the best agreement between experimental UV/Vis absorption spectra and calculated ones (see Figure 12). For clarity, phenyl groups are shown instead of the trialkylphenyl groups. The geometry parameters are $\alpha_1 = \alpha_2 = 70^\circ$, $\beta = 55^\circ$ and a center-to-center distance of 3.5 Å between the molecules. See ref. [39].

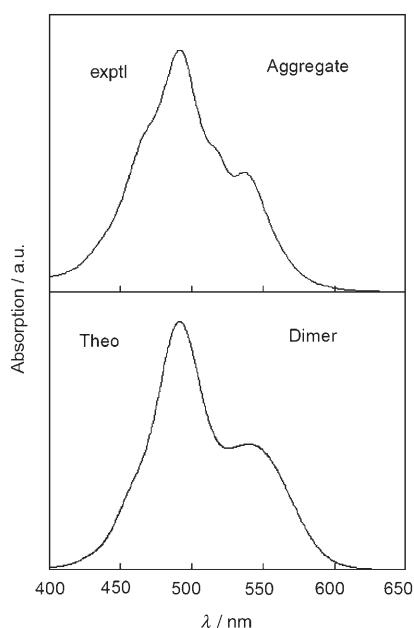


Figure 12. UV/Vis spectrum of **2** measured at 2.2×10^{-4} M in MCH ($\alpha_{\text{agg}} = 0.96$, top) and the calculated dimer spectrum (bottom).

lower panel of Figure 12 is obtained. The spectrum is determined for the case of a low resolution, taking the influence of the surroundings into account. Considering the simplicity of the employed model, the agreement with the experimental spectrum (upper panel) is excellent. Noteworthy, that the extension of the model to a trimer with the same geometric parameters yields absorption spectra similar to that of the dimer, thus, it can be anticipated that the dimer model already provides valuable information about the geometry of the extended oligomeric aggregate.

For cofacial π - π stacks with rotational displacements between the chromophores, photoluminescence can be observed; however, the exciton theory cannot properly describe the emission properties of the aggregates of **2**.^[39] The calculated emission spectrum remarkably differs from the measured one, pinpointing a relaxation process into an emissive state that is different from the Franck-Condon state. Indeed, the observed spectra exhibit features that are similar to those typically observed for excimers,^[41] that is, a structureless broad band with pronounced bathochromic shift and much longer lifetime compared to the monomer species.

Unlike typical excimers where π - π aggregates are formed only in the excited states, while the ground state interactions between the π -systems are repulsive (dissociative), extended 1D π stacks are already given for **2** in the ground state, as shown by NMR, UV/Vis and AFM studies. The formation of excimer-type excited state dimer is, however, feasible. As suggested in Figure 13, upon photoexcitation, pronounced structural and energetic reorganization processes may take place between the excited molecule and the neighbor one to form a relaxed state (MM*) from which emission takes place. Owing to the resonance contributions of exciton and

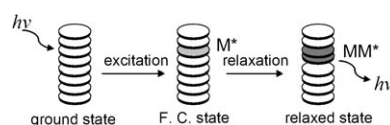


Figure 13. Schematic representation of the excimer formation in the extended π - π stacks of dye **2**.

charge transfer states,^[40] the π - π distance is reduced in this relaxed structure in comparison with that of the ground state π - π stacks. Like the conventional excimers, emission from such excited state dimer will lead to a high energy vibrational level on the ground state potential surface, thus, it has some dissociative character according to the definition of Birks.^[41]

However, despite similarities, there are also differences compared with conventional excimers like those of pyrene in solution.^[41d] First, while the diffusion-controlled collision excimer formation is only feasible at higher concentration or for long-lived excited state species like pyrene,^[42] the probability for the relaxation into a excimer-type emissive state is highly increased by the extended π - π stacking of dye **2** that only requires small displacements between the molecules to give an excited state dimeric unit (Figure 13). Second, the excimer-type band of dye **2** is not totally structureless (Figure 10) in contrast with the unstructured pyrene excimer emission that has been ascribed to the rapid dissociation of the dimer at a repulsive ground state before the molecules can complete a vibration cycle.^[42] In the case of dye **2**, dissociation of the molecules in the ground state is replaced by a structural reorganization into an attractive π - π stacked state. As a result, the vibronic structure can still be observed in contrast to the pyrene excimer band. Indeed, the fluorescence band of concentrated solutions and thin films of **2** can be resolved into several overlapped Gaussian bands with energy interval of 1100–1300 cm^{-1} (Figure S8 in the Supporting Information). Third, the stabilization of the excited dimer unit of strongly quadrupolar perylene bisimide dye **2** might be different from those of pure polycyclic aromatic hydrocarbons like pyrene or perylene. For perylene excimers, it has been reported that exciton interaction and charge transfer interaction have 70 and 30% contribution, respectively, to the total stabilization energy.^[43] For excited aggregates of PBI dye **2**, charge transfer interactions could have a significantly higher contribution due to the presence of two electron acceptor imide groups that embed the electron-rich central perylene unit. Indeed, according to our calculations (Figure 11) already in the ground state the symmetry is broken with one imide acceptor group positioned more on top of the central perylene core than for the other. Thus, it is very likely that the excited aggregates of **2** emanate some properties of charge-transfer excitons.^[44]

As a consequence of such severe structural reorganizations in the excited state, energy transfer process, such as exciton hopping^[45] to nearest neighbor molecules should be slowed down significantly within the extended π - π stacks of these dyes.^[46] Excited dimer species are expected to behave

as traps, which should reduce the exciton mobility compared with ordered one-dimensional stacks and limit the performance of liquid crystalline materials compared to their crystalline counterparts (in organic crystals, the excimers have been recognized as a sort of self-trapped excitons^[47]).

Charge transport properties of PBI 2: The semiconductive properties of present PBI 2 were explored by using the pulse-radiolysis time-resolved microwave conductivity (PR-TRMC) technique.^[48] This technique probes the (change in) conductivity of solid samples upon the generation of charge carriers by irradiation of the sample with high energy electron pulses. In this way, the motion of charge carriers can be probed within solid samples of organic materials without employing electrodes. Since both positive and negative charges are generated during the high energy pulse, it is not possible to distinguish between the contribution of positive and negative charges to the observed conductivity. The conductivity of 2 in a temperature range from room temperature to 380 K is shown in Figure 14. The conductivity was found to decrease by more than an order of magnitude upon the transition from the crystalline phase to the LC phase, as observed for other LC organic materials.^[48b]

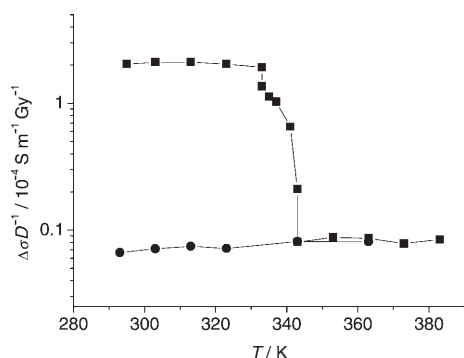


Figure 14. Temperature dependence of the dose-normalized conductivity of PBI 2 for increasing temperature (■) and decreasing temperature (●).

In accordance with our DSC study, no increase of the conductivity could be observed upon cooling because the LC phase prevails. An estimate for the lower limit of the mobility of charge carriers can be made by assuming that all the charges generated during the high energy pulse contribute to the conductivity signal. For this situation, and assuming charge carriers transport in three dimensions, a lower limit of the mobility of 0.047 and 0.0026 cm² V⁻¹ s⁻¹ is calculated for the crystalline phase and the LC phase of 2, respectively. However, our packing model derived from X-ray analysis suggests that the pathways for charge carrier motion along the stacks of the PBI 2 dye is one-dimensional. As a consequence, the mobility for 2 is not isotropic and the mobility value of interest is the mobility along the stacking direction of the dye. Thus, the lower limits of the one-dimensional mobility are 0.14 and 0.0078 cm² V⁻¹ s⁻¹ for the crystalline phase and the LC phase of 2, respectively (Table 2). Further-

Table 2. Charge carrier mobilities of PBI 2 in crystalline and LC phases.

Phase	$\Sigma\mu_{\text{min,iso}}^{[a]}$ [cm ² V ⁻¹ s ⁻¹]	$\Sigma\mu_{\text{min,1D}}^{[a]}$ [cm ² V ⁻¹ s ⁻¹]	$\Sigma\mu_{\text{TRMC,iso}}^{[b]}$ [cm ² V ⁻¹ s ⁻¹]	$\Sigma\mu_{\text{TRMC,1D}}^{[b]}$ [cm ² V ⁻¹ s ⁻¹]
crystal	0.047	0.14	0.14	0.42
LC phase	0.0026	0.0078	0.0076	0.023

[a] $\Sigma\mu_{\text{min,iso}} = \Delta\sigma/D_{\text{cop}} \cdot E_p \cdot (1/f)$, [b] $\Sigma\mu_{\text{TRMC,iso}} = \Delta\sigma/D_{\text{cop}} \cdot E_{p(\text{side chain} = 25 \text{ eV})} \cdot (1/f) \cdot (1/W_{\text{cop}})$. $\Delta\sigma/D_{\text{cop}}$ = charge in conductivity at the end of the pulse, E_p = energy needed to create one electron hole pair, f = fill factor = mass of compound/volume holder, $W_{\text{cop}} = W_s \cdot \text{fraction of charges created in side chains}$.

more, not all generated charges contribute to the conductivity signal and the actual mobility value can be obtained by considering the charge carrier decay during the high-energy electron pulse. Taking these effects into account, the one-dimensional TRMC mobility calculated for PBI 2 in the crystalline phase is 0.42 cm² V⁻¹ s⁻¹. This mobility value is among the best values for molecular semiconductors and compares well with that of another PBI dye reported previously.^[7] Marder and co-workers have recently reported on the charge carrier mobility of the tridodecyloxyphenyl-substituted PBI 1 in the LC phase measured by SCLC and TRMC techniques.^[15d] With SCLC method a mobility value of 0.2 cm² V⁻¹ s⁻¹ was obtained for the LC phase of PBI 1, whereas by TRMC method a mobility of 0.0078 cm² V⁻¹ s⁻¹ was assessed. The latter value is comparable with the lower limit of the mobility (0.0026 cm² V⁻¹ s⁻¹) that we have observed for PBI 2 in the LC phase by TRMC. Obviously, the TRMC mobility cannot be directly compared with the mobility determined by SCLC as significantly different mobility values were found for the same system (LC phase of PBI 1) with these two different techniques.^[15d]

On transformation of the crystalline to the LC phase the structural disorder in the material increases which leads to a reduction in the mobility. At this point we like to speculate that the lowering of the charge carrier mobility in LC phase of PBI 2 is at least partly due to the formation of dimeric traps that are of similar nature as the exciton traps discussed before. The formation of π dimers from radical cationic and anionic species has been amply discussed in the literature, respectively, for oligothiophene and naphthalene bisimide semiconductors in solution and amorphous solid state,^[49] but to our knowledge this discussion has never been extended to liquid crystalline semiconductors, despite their obvious π - π -stacked nature which requires only minor structural reorganization to provide a localized more stable dimeric species. Because such dimeric species (of polaronic or bipolaronic nature) constitute traps, they offer a reasonable explanation for the lower charge carrier mobilities of LC compared to crystalline phases. Thus, the polaronic hopping mobility can be described by the Equation (3)

$$\mu = \frac{A}{T^{3/2}} \exp\left(-\frac{\lambda}{4kT}\right) \quad (3)$$

where A is a constant and λ the reorganization energy.^[50] As the lowest energy absorption of the aggregates of PBI 2

occurs at around 540 nm (Figure 3) and the excimer fluorescence is observed at about 680 nm (Figure 10), a spectral shift of about 0.5 eV is given which can be taken as an approximation for the reorganization energy of a charge carrier. For a reorganization energy of 0.5 eV, the polaronic hopping mobility increases approximately by a factor of 2 upon increasing the temperature from 280 to 380 K. This temperature dependence is only slightly stronger than for the observed mobilities in the LC phase of PBI **2** (Figure 14, circles). Taking into consideration the simplicity of the polaronic hopping model for a description of charge transport, the agreement between the theoretical and measured temperature dependence is fairly good. At higher temperatures enhanced dynamic structural fluctuations may have a negative effect on the mobility, which partially compensates the thermally activated behavior, as expected on the basis of polaronic hopping motion only.

Conclusion

A new, highly soluble PBI dye **2** formed extended fluorescent aggregates in nonpolar solvent. The aggregation behavior is concentration and temperature-dependent and can be described very well with the isodesmic model. Furthermore, dye **2** possesses liquid crystalline properties. Thus, in condensed state a hexagonal columnar LC phase was observed and well-defined columnar nanostructures could be obtained by simple solution casting. X-ray diffraction and AFM studies indicated that the columnar stacking is accomplished by rotational displacement among the molecules which is additionally substantiated by theoretical calculations. Such unique π - π stacking of **2** leads to rather interesting and remarkable absorption and emission properties of the dye aggregates indicating strong electronic coupling and charge transfer interaction among the self-assembled dyes. PR-TRMC conductivity measurements revealed that dye **2** is among the best molecular semiconductors in the crystalline columnar phase. Consequently, the fluorescent nanowires of this dye are ideal candidates for further investigations as n-type semiconducting materials and self-assembled nanoemitters.

Experimental Section

General methods: NMR spectra were recorded at 300 K on Bruker Avance 400 (400 MHz) or DMX 600 (600 MHz, for temperature dependent measurements) spectrometers and the spectra were calibrated against TMS ($\delta=0.0$ ppm). For the temperature-dependent measurements the spectra were calibrated against the chemical shift of residual methylcyclohexane (MCH) in $[D_{14}]MCH$ at $\delta=1.60$ ppm. The solvents for spectroscopic studies were of spectroscopic grade and used as received. UV/Vis spectra were measured on Perkin-Elmer Lambda 40P spectrometer equipped with a Peltier system as temperature controller. Differential scanning calorimetry (DSC) measurements were performed by using a TA Q1000 calorimeter. Optical textures at crossed polarizers were obtained with an Olympus BX-41 polarization microscope equipped with a Linkam THMS 600 hot stage and a temperature controller unit.

Wide angle X-ray diffractograms were obtained at room temperature on a Siemens powder diffractometers ($Cu_{K\alpha}$ radiation). The vapor pressure osmometry measurements were performed on a KNAUER osmometer with a universal temperature measurement unit. Benzil was used as standard and a calibration curve for each temperature (40, 50 and 60°C) in terms of R in Ohm versus molal osmotic concentration (moles per kg MCH) was constructed up to 0.01 molal.

DOSY NMR spectroscopy: 1H DOSY measurements were performed at 298 K on a Bruker DMX 600 (600 MHz) NMR spectrometer equipped with a BGPA 10 gradient generator, a BGU II control unit and a conventional 5 mm broad band ($^{15}N, ^{31}P$)/ 1H probe with z axis gradient coil capable of producing pulsed magnetic field gradients in the z direction of 52 G cm^{-1} . The NMR spectra were recorded in $[D_{14}]MCH$ solutions in 5 mm Norell NMR tubes. The spectral data were acquired using the longitudinal eddy current delay sequence with bipolar gradient pulse pairs for diffusion (BPP-LED)^[51] and additional sinusoidal spoil gradients after the second and fourth 90° pulses were used. The temperatures were calibrated with a probe of 4% MeOH in CD_3OD . The fluctuation of the temperature was less than 0.1 K during the measurements. The strength of the pulsed magnetic field gradients was calibrated by 1H DOSY experiments with a sample of 1% H_2O in 99% D_2O , doped with $GdCl_3$ (0.1 mg per mL) to achieve short spin-lattice relaxation times, using the known value of the diffusion coefficient for H_2O at 298 K in this H_2O/D_2O mixture. The diffusion coefficient D was obtained by curve fitting according to the equation $I = I_0 \exp[-D\gamma^2 g^2 \delta^2 (\Delta - \delta/3)]$, where I is the observed intensity for the gradient strength g and γ is the gyromagnetic ratio of the observed nuclei, Δ represents the diffusion time reduced by half of the delay ($\tau=300\text{ }\mu s$) between the two gradients of a bipolar gradients pulse pair and δ is the duration of the short bipolar gradient pulses. For each spectrum, the average value of D obtained from different aromatic signals (at least 3, depending on the numbers of the aromatic signals) was used.

Fluorescence measurements: The steady state fluorescence spectra and the fluorescence anisotropy were measured under ambient conditions on a PTI QM4/2003 spectrofluorometer equipped with two Glan-Thomson polarizers under magic angle and front-face setup due to the high optical density of the samples. All the fluorescence spectra were corrected. The fluorescence quantum yields were determined by the optical dilution method using fluorescein ($\Phi_f=0.92$ in 1N aqueous NaOH) as standard.^[52] The given quantum yields are averaged value of data obtained at three different excitation wavelengths. The fluorescence anisotropy r is defined as $r = (I_{VV} - GI_{VH}) / (I_{VV} + 2GI_{VH})$, where $G = I_{HV}/I_{HH}$ and I is the fluorescence intensity at a specific wavelength and the indices are related to the vertical or horizontal orientation of the excitation (first index) and the emission polarizer (second index) with respect to the excitation-emission plane. G is an instrument factor which compensates for polarization effects of the emission optics. Correction for the G factor was obtained automatically. Fluorescence intensities were averaged for 60 s at 2 points per s, bandpass was set to 6 nm, and the measurements were performed at room temperature.

Fluorescence lifetimes were measured under ambient conditions according to the method described in the literature.^[53] By using a PTI Laser-Strobe fluorescence lifetime spectrometer system containing a GL-3300 nitrogen laser (337.1 nm, pulse width 600 ps, pulse energy 1.45 mJ) coupled with a dye laser GL-302 (pulse width 500 ps, pulse energy 220 μJ at 550 nm) as an excitation source and a stroboscopic detector. Laser output was tuned within the emission curves of the laser dyes supplied by the manufacturer (PLD 421, 500, 579, 665, 735). The time resolution following deconvolution of experimental decays was 200 ps. The instrument response function was collected by scattering the exciting light of a dilute, aqueous suspension of colloidal silica (Ludox). Decay curves were evaluated using the software supplied with the instrument applying least square regression analysis. The quality of the fit was evaluated by analysis of χ^2 (0.9–1.1), DW factor (> 1.75) and Z value (< -1.96 , confidence level 0.95) as well as by inspection of residuals and autocorrelation function.

Atomic force microscopy (AFM): AFM measurements were performed under ambient conditions using a MultiMode Nanoscope IV system oper-

ating in tapping mode in air. Silicon cantilevers (OMCL-AC160TS) with a resonance frequency of ≈ 300 kHz were used. Solution of perylene bisimide **2** in MCH was spin-coated onto a HOPG (highly ordered pyrolytic graphite) under 7000 rpm.

Charge carrier mobility measurements: The conductive properties were studied with the pulse-radiolysis time-resolved microwave conductivity (PR-TRMC) technique. Pressed pellets (25 mg, fill factor 0.75) of the material were irradiated with 10 nanosecond pulses of 3 MeV electrons from a Van de Graaff accelerator, which results in the creation of a uniform micromolar concentration of electron-hole pairs. The resulting change in conductivity was monitored as the microwave power absorbed by the mobile charge carriers in the material at an electro-magnetic field frequency of 33 GHz. The mobility values were determined from the conductivity at the end of the electron pulse. The lower limit to the mobility was obtained by assuming that all generated charges contribute to the conductivity (survival parameter $W_{\text{cop}} = 1$) and a pair formation energy of 16 eV. This pair formation energy was obtained using the electron density fractions (f) and the pair formation energies (E_p) of the side chains ($f = 0.79$, E_p 25 eV) and the core of the dye ($f = 0.21$, $E_p = 6.72$ taken from the onset of optical absorption) as described elsewhere.^[48] The one-dimensional TRMC mobility was calculated assuming that electron-hole pairs generated in the core of the dye recombine and that only a fraction of charges generated in the side chains (W_s) escapes recombination. For compound **2** an escape fraction W_s of 0.72 can be determined.^[54] Using the electron density fractions mentioned above, the fraction of the charges that contributes to the conductivity signal W_{cop} was 0.54. The mobility data for PBI **2** are collected in Table 2.

3,4,5-Tris(1'-dodecynyl)-nitrobenzene (5): 3,4,5-Triodonitrobenzene (3.0 g, 6.0 mmol), bis(triphenylphosphine)-palladium(II) dichloride (252 mg, 0.30 mmol), copper(I) iodide (115 mg, 0.60 mmol) were mixed in triethylamine (80 mL) under argon atmosphere and stirred at 80 °C. Then 1-dodecynene (3.30 g, 19.8 mmol) was added dropwise and the reaction mixture was stirred for another 4 h. After cooling to room temperature, the solid precipitate was removed by filtration and the solution was concentrated by rotary evaporation. The residue was purified by silica gel column chromatography with *n*-hexane/acetone 10:1 to obtain a brown oil (3.40 g, 93 %). ¹H NMR (400 MHz, CDCl₃, 300 K, TMS): δ = 8.08 (s, 2H, Ar-H), 2.54 (t, 2H, $J = 7.0$ Hz, C \equiv CCH₂), 2.46 (t, 4H, $J = 7.0$ Hz, C \equiv CCH₂), 1.65 (m, 6H, CH₂), 1.49 (m, 6H, CH₂), 1.4–1.1 (m, 36H, CH₂), 0.88 (m, 9H, CH₃); MS (EI, 70 eV): m/z (%): 615.6 (100) [M]⁺; elemental analysis (%) calcd for C₄₂H₆₅NO₂ (616.0): C 81.90, H 10.64, N 2.27; found: C 81.50, H 11.05, N 2.36.

3,4,5-Tridodecylaniline (6): 3,4,5-Tri(1'-dodecynyl)-nitrobenzene (1.60 g, 2.60 mmol) was placed in a flask containing 10 % Pd/C (0.4 g) and dry ethanol (80 mL) and dry ethyl acetate (20 mL). The flask was affixed with balloons filled with hydrogen gas and the mixture was stirred at room temperature for 24 h. Then the Pd/C in the reaction mixture was removed by filtration and the solvent was removed by rotary evaporation. The resulting brown oil was purified by silica gel column chromatography with *n*-hexane/CH₂Cl₂ 1:1 to give slightly yellow oil which became a white solid when stored in refrigerator (0.96 g, 53 %). ¹H NMR (400 MHz, CDCl₃, 300 K, TMS): δ = 6.41 (s, 2H, Ar-H), 2.48 (m, 6H, Ar-CH₂), 1.7–1.1 (m, 60H, CH₂), 0.88 (m, 9H, CH₃), a very broad signal was observed for NH₂ protons at 4.0–3.0 ppm; MS (EI, 70 eV): m/z (%): 598.1 (100) [M]⁺; elemental analysis (%) calcd for C₄₂H₇₀N (598.1): C 84.34, H 13.31, N 2.34; found: C 84.37, H 13.32, N 2.32.

***N,N'*-Di(3,4,5-tridodecylphenyl)-perylene-3,4,9,10-tetracarboxylic acid bisimide (2):** A mixture of perylene-3,4,9,10-tetracarboxylic acid bisanhydride (0.13 g, 0.33 mmol), aniline **6** (0.40 g, 0.67 mmol) and zinc acetate (0.073 g, 0.33 mmol) were mixed in quinoline (15 mL). The reaction mixture was stirred at 180 °C for 2 h. After cooling to room temperature, the mixture was poured into MeOH (30 mL). The precipitate was collected by filtration, washed with methanol (3 \times 20 mL), and then dried in vacuum. The crude product was further purified by silica gel column chromatography (CH₂Cl₂) and then slowly precipitated from CH₂Cl₂/methanol 1:1 (10 mL) to give a red powder (280 mg, 56 %). ¹H NMR (400 MHz, CDCl₃, 300 K, TMS): δ = 8.74 (d, 4H, $J = 8.0$ Hz, H_{peryl}), 8.66 (d, 4H, $J = 8.2$ Hz, H_{peryl}), 6.97 (s, 4H, Ar-H), 2.66 (m, 12H, Ar-CH₂), 1.8–

1.2 (m, 120H, CH₂), 0.88 (m, 18H, CH₃); MS (FAB, matrix: *p*-octyloxynitrobenzene): m/z : calcd for C₁₀₈H₁₆₂N₂O₄: 1551.3; found: 1551.2 [M]⁺; elemental analysis (%) calcd for C₁₀₈H₁₆₂N₂O₄ (1552.5): C 83.56, H 10.52, N 1.80; found: C 83.13, H 10.75, N 1.89; UV/Vis (CH₂Cl₂): λ_{max} (ϵ) = 527 (96300), 491 (58100), 460 (21000), 434 (6100), 369 (5000 mol⁻¹ L cm⁻¹); fluorescence (CH₂Cl₂): λ_{max} = 532 nm; quantum yield: Φ_f = 0.63.

Acknowledgements

We are grateful to the Deutsche Forschungsgemeinschaft for financial support for this work within the research graduate school GK 1221 "Control of electronic properties of aggregates of π -conjugated molecules" at the University of Würzburg. We are indebted to Dr. Matthias Grüne and Elfriede Ruckdeschel for the DOSY NMR measurements, Professor R. B. Neder for XRD measurements, and their helpful discussions.

- a) F. J. M. Hoebe, P. Jonkheijm, E. W. Meijer, A. P. H. J. Schenning, *Chem. Rev.* **2005**, *105*, 1491–1546; b) *Supramolecular Dye Chemistry*, Vol. 258 (Ed.: F. Würthner), Topics in Current Chemistry, Springer, Berlin, **2005**.
- a) T. Pullerits, V. Sundstrom, *Acc. Chem. Res.* **1996**, *29*, 381–389; b) T. S. Balaban, H. Tamiaki, A. R. Holzwarth, *Top. Curr. Chem.* **2005**, *258*, 1–38; c) X. Hu, T. Ritz, A. Damjanovic, F. Autenrieth, K. Schulten, *Q. Rev. Biophys.* **2002**, *35*, 1–62.
- a) W. Pisula, M. Kastler, D. Wasserfallen, J. W. F. Robertson, F. Nolde, C. Kohl, K. Müllen, *Angew. Chem.* **2006**, *118*, 834–838; *Angew. Chem. Int. Ed.* **2006**, *45*, 819–823; b) J. P. Hill, W. Jin, A. Kosaka, T. Fukushima, H. Ichihara, T. Shimomura, K. Ito, T. Hashizume, N. Ishii, T. Aida, *Science* **2004**, *304*, 1481–1483.
- a) T. van der Boom, R. T. Hayes, Y. Zhao, P. Bushard, E. A. Weiss, M. R. Wasielewski, *J. Am. Chem. Soc.* **2002**, *124*, 9582–9590; b) F. Würthner, Z. Chen, F. J. M. Hoebe, P. Osswald, C.-C. You, P. Jonkheijm, J. v. Herrikhuyzen, A. P. H. J. Schenning, P. P. A. M. van der Schoot, E. W. Meijer, E. H. A. Beckers, S. C. J. Meskers, R. A. J. Janssen, *J. Am. Chem. Soc.* **2004**, *126*, 10611–10618; c) M. G. Debijs, Z. Chen, J. Piris, R. B. Neder, M. M. Watson, K. Müllen, F. Würthner, *J. Mater. Chem.* **2005**, *15*, 1270–1276.
- F. Würthner, *Chem. Commun.* **2004**, 1564–1579 and references therein.
- H. Langhals, J. Karolin, L. B. Johansson, *J. Chem. Soc. Faraday Trans.* **1998**, *94*, 2919–2922.
- C. W. Struijk, A. B. Sieval, J. E. J. Dakhurst, M. Dijk, P. Kimkes, R. B. M. Koehorst, H. Donker, T. J. Schaafsma, S. J. Picken, A. M. van de Craats, J. M. Warman, H. Zuilhof, E. J. R. Sudhölter, *J. Am. Chem. Soc.* **2000**, *122*, 11057–11066.
- a) F. C. DeSchryver, T. Vosch, M. Cotlet, M. van der Auweraer, K. Müllen, J. Hofkens, *Acc. Chem. Res.* **2005**, *38*, 514–522; b) A. Sautter, B. K. Kaletas, D. G. Schmid, R. Dobrawa, M. Zimine, G. Jung, I. H. M. Van Stokkum, L. De Cola, R. M. Williams, F. Würthner, *J. Am. Chem. Soc.* **2005**, *127*, 6719–6729; c) T. Ishi-i, K. Murakami, Y. Imai, S. Mataka, *Org. Lett.* **2005**, *7*, 3175–3178.
- a) M. P. O'Neil, M. P. Niemczyk, W. A. Svec, D. Gosztola, G. L. Gaines III, M. R. Wasielewski, *Science* **1992**, *257*, 63–65; b) E. H. A. Beckers, S. C. J. Meskers, A. P. H. J. Schenning, Z. Chen, F. Würthner, R. A. J. Janssen, *J. Phys. Chem. A* **2004**, *108*, 6933–6937; c) A. Prodi, C. Chiorboli, F. Scandola, E. Iengo, E. Alessio, R. Dobrawa, F. Würthner, *J. Am. Chem. Soc.* **2005**, *127*, 1454–1462.
- a) A. Kraft, A. C. Grimsdale, A. B. Holmes, *Angew. Chem.* **1998**, *110*, 416–443; *Angew. Chem. Int. Ed.* **1998**, *37*, 402–428; b) C. Karapire, C. Zafer, S. Icli, *Synth. Met.* **2004**, *145*, 51–60; c) J. Pan, W. Zhu, S. Li, W. Zeng, Y. Cao, H. Tian, *Polymer* **2005**, *46*, 7658–7669.
- a) P. R. L. Malenfant, C. D. Dimitrakopoulos, J. D. Gelorme, L. L. Kosar, T. O. Graham, *Appl. Phys. Lett.* **2002**, *2517*–2519; b) C. D. Dimitrakopoulos, P. R. L. Malenfant, *Adv. Mater.* **2002**, *14*, 99–117; c) B. A. Jones, M. J. Ahrens, M.-H. Yoon, A. Facchetti, T. J. Marks, M. R. Wasielewski, *Angew. Chem.* **2004**, *116*, 6523–6526; *Angew.*

- Chem. Int. Ed.* **2004**, *116*, 6363–6366; d) for a recent review, see: F. Würthner, R. Schmidt, *ChemPhysChem* **2006**, *7*, 793–797.
- [12] a) C. W. Tang, *Appl. Phys. Lett.* **1986**, *48*, 183–185; b) L. Schmidt-Mende, A. Fechtenkötter, K. Müllen, E. Moons, R. H. Friend, J. D. MacKenzie, *Science* **2001**, *293*, 1119–1122; c) A. J. Breeze, A. Salomon, D. S. Ginley, B. A. Gregg, H. Tillmann, H.-H. Hörhold, *Appl. Phys. Lett.* **2002**, *81*, 3085–3087.
- [13] A. Tracz, J. K. Jeszka, M. D. Watson, W. Pisula, K. Müllen, T. Pakula, *J. Am. Chem. Soc.* **2003**, *125*, 1682–1683.
- [14] P. Jonkhøj, F. J. M. Hoeben, R. Kleppinger, J. van Herrikhuyzen, A. P. H. J. Schenning, E. W. Meijer, *J. Am. Chem. Soc.* **2003**, *125*, 15941–15949.
- [15] a) F. Würthner, C. Thalacker, S. Diele, C. Tschierske, *Chem. Eur. J.* **2001**, *7*, 2245–2253; b) I. K. Iverson, S. M. Casey, W. Seo, S.-W. Tam-Chang, B. A. Pindzola, *Langmuir*, **2002**, *18*, 3510–3516; c) J. van Herrikhuyzen, A. Syamakumari, A. P. H. J. Schenning, E. W. Meijer, *J. Am. Chem. Soc.* **2004**, *126*, 10021–10027; d) Z. An, J. Yu, S. C. Jones, S. Barlow, S. Yoo, B. Domercq, P. Prins, L. D. A. Siebbeles, B. Kippelen, S. R. Marder, *Adv. Mater.* **2005**, *17*, 2580–2583.
- [16] J. M. Warman, A. M. Van De Craats, *Mol. Cryst. Liq. Cryst.* **2003**, *396*, 41–72.
- [17] A. Bayer, J. Hübner, J. Kopitzke, M. Oestreich, W. Rühle, J. H. Wendorff, *J. Phys. Chem. A* **2001**, *105*, 4596–4602.
- [18] a) C. Tschierske, *J. Mater. Chem.* **1998**, *8*, 1485–1508; b) C. D. Simpson, J. Wu, M. D. Watson, K. Müllen, *J. Mater. Chem.* **2004**, *14*, 494–504.
- [19] M. O. Vysotsky, V. Böhmer, F. Würthner, C.-C. You, K. Rissanen, *Org. Lett.* **2002**, *4*, 2901–2904.
- [20] E. H. A. Beckers, S. C. J. Meskers, A. P. H. J. Schenning, Z. Chen, F. Würthner, R. A. J. Janssen, *J. Phys. Chem. A* **2004**, *108*, 6933–6937.
- [21] F. Würthner, Z. Chen, V. Dehm, V. Stepanenko, *Chem. Commun.* **2006**, 1188–1190.
- [22] a) R. Singh, G. Just, *J. Org. Chem.* **1989**, *54*, 4453–4457; b) H.-C. Zhang, W.-S. Huang, L. Pu, *J. Org. Chem.* **2001**, *66*, 481–487; c) S. Thorand, N. Krause, *J. Org. Chem.* **1998**, *63*, 8551–8553; d) M. Sonoda, A. Inaba, K. Itahashi, Y. Tobe, *Org. Lett.* **2001**, *3*, 2419–2421.
- [23] C. Niemann, C. E. Redemann, *J. Am. Chem. Soc.* **1941**, *63*, 1549–1552.
- [24] H. Langhals, *Chem. Ber.* **1985**, *118*, 4540–4543.
- [25] a) J. Hofkens, T. Vosch, M. Maus, F. Köhn, M. Cotlet, T. Weil, A. Herrmann, K. Müllen, F. C. De Schryver, *Chem. Phys. Lett.* **2001**, *333*, 255–263; b) S. K. Lee, Y. Zu, A. Herrmann, Y. Geerts, K. Müllen, A. J. Bard, *J. Am. Chem. Soc.* **1999**, *121*, 3513–3520.
- [26] W. Wang, J. J. Han, L.-Q. Wang, L.-S. Li, W. J. Shaw, A. D. Q. Li, *Nano Lett.* **2003**, *3*, 455–458.
- [27] For reviews on this technique, see: a) C. S. Johnson Jr., *Prog. Nucl. Magn. Reson. Spectrosc.* **1999**, *34*, 203–256; b) Y. Cohen, L. Avram, L. Frish, *Angew. Chem.* **2005**, *117*, 524–560, *Angew. Chem. Int. Ed.* **2005**, *44*, 520–554.
- [28] a) W. S. Price, Fumihiko, Tsuchiya, Y. Arata, *J. Am. Chem. Soc.* **1999**, *121*, 11503–11512; b) W. S. Price in *Encyclopaedia of Nuclear Magnetic Resonance*, Vol. 9 (Eds.: D. M. Grant, R. K. Harris), Wiley, West Sussex, **2002**, pp. 364–373.
- [29] The formation of dimer or higher aggregates not only depends on the intrinsic properties of the molecules, but also on external conditions, that is, temperature, solvent, pH value of the environment, etc.; for examples of distinct monomer–dimer equilibria of dye aggregates, see: a) A. S. Shetty, J. Zhang, J. S. Moore, *J. Am. Chem. Soc.* **1996**, *118*, 1019–1027; b) F. Würthner, S. Yao, T. Debaeremaeker, R. Wortmann, *J. Am. Chem. Soc.* **2002**, *124*, 9431–9447; c) J. Wu, A. Fechtenkötter, J. Gauss, M. D. Watson, M. Kastler, C. Fechtenkötter, M. Wagner, K. Müllen, *J. Am. Chem. Soc.* **2004**, *126*, 11311–11321. For examples of oligomeric or polymeric dye aggregates, see: d) A. W. Snow, N. L. Jarvis, *J. Am. Chem. Soc.* **1984**, *106*, 4706–4711; R. E. Hughes, S. P. Hart, D. A. Smith, B. Movaghar, R. J. Bushby, N. Boden, *J. Phys. Chem. A* **2002**, *106*, 6638–6645.
- [30] R. Dobrawa, M. Lysetska, P. Ballester, M. Grüne, F. Würthner, *Macromolecules* **2005**, *38*, 1315–1325.
- [31] B. C. Burdett, *Studies in Physical and Theoretical Chemistry*, **1983**, *26* (Aggregation Processes in Solution), 241–270.
- [32] M. Sadrai, L. Hadel, R. R. Sauer, S. Husain, K. Krogh-Jespersen, J. D. Westbrook, G. R. Bird, *J. Phys. Chem.* **1992**, *96*, 7988–7996.
- [33] a) R. B. Martin, *Chem. Rev.* **1996**, *96*, 3043–3064; b) N. J. Baxter, M. P. Williamson, T. H. Lilley, E. Haslan, *J. Chem. Soc. Faraday Trans. 2* **1996**, *92*, 231–234; c) *Supramolecular polymers* (Ed.: A. Ci ferri), CRC Press, Boca Raton, **2005**; d) P. van der Schoot, M. A. J. Michels, L. Brunsveld, R. P. Sijbesma, A. Ramzi, *Langmuir* **2000**, *16*, 10076–10083.
- [34] A. P. H. J. Schenning, P. Jonkhøj, E. Peeters, E. W. Meijer, *J. Am. Chem. Soc.* **2001**, *123*, 409–416.
- [35] V. Percec, C.-H. Ahn, T. K. Bera, G. Ungar, D. J. P. Yearley, *Chem. Eur. J.* **1999**, *5*, 1070–1083.
- [36] a) F. Graser, E. Hädicke, *Liebigs Ann. Chem.* **1980**, 1994–2011; b) G. Klebe, F. Graser, E. Hädicke, J. Berndt, *Acta Crystallogr. Sect. B* **1989**, *45*, 69–77; c) P. Zugenmaier, J. Duff, T. L. Bluhm, *Cryst. Res. Technol.* **2000**, *35*, 1095–1115.
- [37] In *n*-hexane, the aggregation constant of dye **2** is $1.2 \times 10^6 \text{ M}^{-1}$ at RT, which is about one order of magnitude higher than that in MCH.
- [38] a) M. Kasha, H. R. Rawls, M. A. El-Bayoumi, *Pure Appl. Chem.* **1965**, *11*, 371–392; b) V. Czikkely, H. D. Försterling, H. Kuhn, *Chem. Phys. Lett.* **1970**, *6*, 207–210; c) P. W. Bohn, *Annu. Rev. Phys. Chem.* **1993**, *44*, 37–60; d) *J-Aggregates* (Ed.: T. Kobayashi), World Scientific, Singapore, **1996**.
- [39] J. Seibt, P. Marquetand, V. Engel, Z. Chen, V. Dehm, F. Würthner, *Chem. Phys.* **2006**, *328*, 354–362.
- [40] a) A. Witkowski, W. Moffit, *J. Chem. Phys.* **1960**, *33*, 872–875; b) R. L. Fulton, M. Goutermann, *J. Chem. Phys.* **1964**, *41*, 2280–2286.
- [41] a) J. B. Birks, *Rep. Prog. Phys.* **1975**, *38*, 903–974; b) S. A. Jenekhe, J. A. Osaheni, *Science*, **1994**, *265*, 765–768; c) B. J. Schwartz, *Annu. Rev. Phys. Chem.* **2003**, *54*, 141–172; d) A. Hayer, V. de Halleux, A. Köhler, A. El-Garouhy, E. W. Meijer, J. Barberá, J. Tant, J. Levin, M. Lehmann, J. Gierschner, J. Cornil, Y. H. Geerts, *J. Phys. Chem. B* **2006**, *110*, 7653–7659.
- [42] N. J. Turro, *Modern Molecular Photochemistry*, University Science Books, Mill-Valley, California, **1991**, pp. 137–143.
- [43] R. Katoh, S. Sinha, S. Murata, M. Tachiya, *J. Photochem. Photobiol. A* **2001**, *145*, 23–34.
- [44] The formation of photoluminescent charge transfer excitons has been reported by Forrest and co-workers for perylene tetracarboxylic dianhydride (PTCDA) crystals. These crystals contain 1D stacks of tightly packed (π – π distance of 3.2 Å) chromophores that facilitate a high degree of π -orbital overlap between adjacent molecules along the stack, see: a) F. F. So, S. R. Forrest, *Mol. Eng. Mol. Cryst. Liq. Cryst. Sci. Technol. Sec. B* **1992**, *2*, 205–222; b) Z. Shen, P. E. Burros, S. R. Forrest, M. Ziari, W. H. Steier, *Chem. Phys. Lett.* **1995**, *236*, 129–134; c) V. Bulovic, P. E. Burrows, S. R. Forrest, J. A. Cronin, M. E. Thompson, *Chem. Phys.* **1996**, *210*, 1–12; d) S. R. Forrest, *Chem. Rev.* **1997**, *97*, 1793–1896.
- [45] L. M. Herz, C. Daniel, C. Silva, F. J. M. Hoeben, A. P. H. J. Schenning, E. W. Meijer, R. H. Friend, *Phys. Rev. B* **2003**, *68*, 045203.
- [46] Bayer, J. Hübner, J. Kopitzke, M. Oestreich, W. Rühle, J. H. Wendorff, *J. Phys. Chem. B* **2001**, *105*, 4596–4602.
- [47] a) A. H. Matsui, *Pure Appl. Chem.* **1995**, *67*, 429–436; b) S. Jurse nas, A. Gruodis, G. Kodis, M. Chachisvilis, V. Gulbinas, E. A. Sil insh, L. Valkunas, *J. Phys. Chem. B* **1998**, *102*, 1086–1094.
- [48] a) P. G. Schouten, J. M. Warman, M. P. de Haas, *J. Phys. Chem.* **1993**, *97*, 9863–9870; b) P. G. Schouten, J. M. Warman, M. P. de Haas, C. F. van Nostrum, G. H. Gelink, R. J. M. Nolte, M. J. Copyn, J. W. Zwikker, M. K. Engel, M. Hanack, Y. H. Chang, W. T. Ford, *J. Am. Chem. Soc.* **1994**, *116*, 6880–6894.
- [49] Formation of π -dimers of oligothiophene radical cations, see: a) M. G. Hill, J. F. Penneau, B. Zinger, K. R. Mann, L. L. Miller, *Chem. Mater.* **1992**, *4*, 1106–1113; b) Y. Yu, E. Gunic, B. Zinger, L. L. Miller, *J. Am. Chem. Soc.* **1996**, *118*, 1013–1018; c) J. A. E. H. van Haare, M. van Bostel, R. A. J. Janssen, *Chem. Mater.* **1998**, *10*, 1166–1175; d) D. A. Scherlis, N. Marzari, *J. Phys. Chem. B*, **2004**,

- 108, 17791–17795; e) T. Sakai, T. Satou, T. Kaikawa, K. Takimiya, T. Otsubo, Y. Aso, *J. Am. Chem. Soc.* **2005**, *127*, 8082–8089; for π -dimers of naphthalene bisimide radical anions, see: f) J.-F. Penneau, B. J. Stallman, P. H. Kasai, L. L. Miller, *Chem. Mater.* **1991**, *3*, 791–796; g) L. L. Miller, K. R. Mann, *Acc. Chem. Res.* **1996**, *29*, 417–423.
- [50] P. Prins, K. Senthikumar, F. C. Grozema, P. Jonkheijm, A. P. H. J.; Schenning, E. W. Meijer, L. D. A. Siebbeles, *J. Phys. Chem. A* **2005**, *109*, 18267–18274.
- [51] D. Wu, A. Chen, C. S. Johnson, *J. Magn. Reson. Ser. A* **1995**, *115*, 260–264.
- [52] J. N. Demas, G. A. Grosby, *J. Phys. Chem.* **1971**, *75*, 991–1024.
- [53] R. G. Bennett, *Rev. Sci. Instrum.* **1960**, *31*, 1275–1279.
- [54] J. M. Warman, K.-D. Asmus, R. H. Schuler, *J. Phys. Chem.* **1969**, *73*, 931–939.
- [55] **Note added in proof:** While this paper was in print, we had the opportunity to perform measurements on a recently developed absolute photoluminescence quantum yield measurement system C9920-02 from Hamamatsu (Japan). For compound **2**, the following absolute quantum yields were determined: 47% for a 0.1 mmol L⁻¹ aggregate solution in *n*-hexane and 16% for thin films. Both values are in good agreement with the results shown in Figure 10 and substantiate our conclusion that a significant photoluminescence is observed from these *H*-type dye aggregates. We are thankful to Dr. Tanja Schüttigkeit and Mr. Hiroyuki Shirai of Hamamatsu Photonics for the opportunity to conduct these measurements with their help in Würzburg.

Received: June 22, 2006

Revised: October 23, 2006

Published online: December 4, 2006